ACCOUNTS of chemical research

Article

pubs.acs.org/accounts

Aromaticity, Closed-Shell Effects, and Metallization of Hydrogen

Ivan I. Naumov[‡] and Russell J. Hemley*[,‡]

Geophysical Laboratory, Carnegie Institution of Washington, 5251 Broad Branch Road NW, Washington, D.C. 20015, United States

Supporting Information

CONSPECTUS: Recent theoretical and experimental studies reveal that compressed molecular hydrogen at 200−350 GPa transforms to layered structures consisting of distorted graphene sheets. The discovery of chemical bonding motifs in these phases that are far from close-packed contrasts with the long-held view that hydrogen should form simple, symmetric, ambient alkali-metal-like structures at these pressures. Chemical bonding considerations indicate that the realization of such unexpected structures can be explained by consideration of simple low-dimensional model systems based on H_6 rings and graphene-like monolayers.

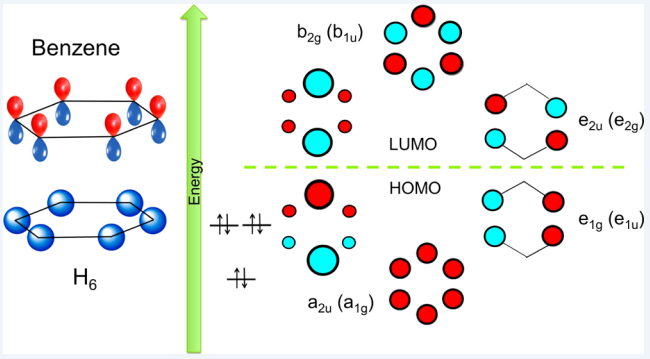

Both molecular quantum chemistry and solid-state physics approaches show that these model systems exhibit a special stability, associated with the completely filled set of bonding orbitals or valence bands. This closed-shell effect persists in the experimentally observed layered structures where it prevents the energy gap from closing, thus delaying the pressure-induced metallization. Metallization occurs upon further compression by destroying the closed shell electronic structure, which is mainly determined by the 1s electrons via lowering of the bonding bands stemming from the unoccupied atomic 2s and 2p orbitals. Because enhanced diamagnetic susceptibility is a fingerprint of aromaticity, magnetic measurements provide a potentially important tool for further characterization of compressed hydrogen. The results indicate that the properties of dense hydrogen are controlled by chemical bonding forces over a much broader range of conditions than previously considered.

INTRODUCTION

The concept of a closed electron shell underlies our understanding of structural stability in chemistry.[1] In atoms and molecules, the closed-shell effect manifests itself in many ways, from the inertness of noble elements to the structure and stability of simple polyatomic molecules like benzene. Similar criteria for stability exist for low-dimensional systems, from two-dimensional thin films[2] to one-dimensional nanowires[3] and zero-dimensional clusters.[4] The simplest chemical system for elucidating this effect is of course the covalent bond of the hydrogen molecule.[5,6] The stability of the small clusters of hydrogen molecules arising from long-range dispersion (van der Waals) interactions has been thoroughly studied and well understood.[7] The energetics of hydrogen molecules and the extent to which the energetics are controlled by chemical (e.g., covalent) bonding has received less attention, in part because of the lack of experimental tests of models over the appropriately large range of interatomic distances in the material.

Recent high-pressure experiments reveal new structures and bonding configurations that appear to challenge conventional chemical rules developed for molecular systems under ambient conditions.[8,9] An example is the surprising new phases of dense molecular hydrogen having anisotropic layered structures[10−17] based on networks of distorted six-membered rings[18−20] that have been discovered at multimegabar (200−350 GPa) pressures (Figure 1). These findings contrast with the original predictions and long-held assumptions that hydrogen forms simple symmetric, close-packed structures at very high densities, as expected from simple physical arguments and observed in alkali metals at ambient conditions.[21] Simulation techniques from condensed-matter physics have successfully predicted aspects of

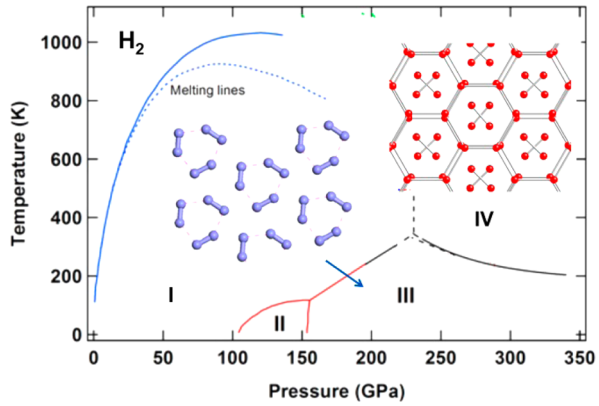

Figure 1. High $P-T$ phase diagram of hydrogen[17] and model structures for the highest pressure phases, the $C2/c$ and $Pbcn$ structures[15,18] for phases III and IV, respectively. Closely related structures are also predicted for these phases (e.g., ref 19).

Received: July 28, 2014
Published: November 4, 2014

   dx.doi.org/10.1021/ar5002654 | Acc. Chem. Res. 2014, 47, 3551−3559

the new structures,[12−16] but the chemical driving force is not readily evident from such calculations.

Here we explore the chemical aspects of the well-known problem behavior of hydrogen at very high densities, including the regime of pressure-induced metallization. This was first articulated in 1935 in the chemistry literature by Wigner and Huntington[21] and motivated in part by Bernal's 1926 conjecture of the stability of valence or metallic lattices at high pressures (see footnote 1 of ref 21). We show that the stability of structures of hydrogen at high pressure can be explained by aromatic or closed-shell effects analogous to those in aromatic hydrocarbons. The new findings arise from seminal studies carried out by Herschbach and co-workers beginning in the late 1970s.[22−24] The implications for those results have been brought into clearer focus with the subsequent discovery of graphene in 2004[25] and newly discovered phases of hydrogen at megabar pressures.[10−19] Whereas most of the theoretical work on hydrogen has been carried out using solid-state physics (i.e., total energy band structure) methods, we show that chemical approaches provide important insights that may be missing from or overlooked in conventional solid state methods. Despite the different approximations used in the two approaches, the key results are independent of the methods used and are obtained from both types of treatments. The results indicate that chemical bonding plays a major role in controlling the properties of hydrogen up to conditions of pressure-induced metallization of the solid.

CLOSED-SHELL INTERACTIONS IN HYDROGEN CLUSTERS

According to Hückel's rule, aromatic compounds must have $4n + 2$ π electrons with $n = 0, 1, 2, 3, ...$ The archetypal example is benzene (C_6H_6), which contains a filled π shell containing six π electrons with one p_z electron on each C atom ($n = 1$). Of the two sets of bonds in benzene, σ and π, it is the σ bonds that are responsible for the symmetric D_{6h} framework with a bond-equalized geometry. The π-component induces a distorted Kekulean geometry, that is, an asymmetrical configuration of three C_2 pairs. Despite this preference, the delocalization of π-electrons produces an extra stabilization in aromatic compounds due to the decrease in resonance energy[26] (Hückel's rule) relative to an interrupted (acyclic) conjugation reference system[27,28] and giving rise to the shortening and lengthening of single and double bonds.[28] Although Hückel's $4n + 2$ rule strictly applies only to regular monocyclic rings, any polycyclic hydrocarbon consisting of C_6 units can also be viewed as aromatic, including its ultimate two-dimensional expression in graphene. Graphene is considered aromatic, as is clear from graphene fragments of increasing size.[29,30]

There is an important analogy between the 1s electrons in hydrogen and the π electrons in carbon. Accordingly, hydrogen chains have been considered for many years as model systems for Hückel's aromatic compounds. Figure 2 shows the analogy between benzene and H_6. In H_n rings, the s electrons play a role similar to that of π-electrons in aromatic compounds, and rings with $n = 6$ and 10 have the first and second lowest energy per atom, respectively.[31,32] Though hydrogen rings containing $4n + 2$ electrons are relatively stable, their energies lie above their ground state dissociation products with localized electrons. The only exception is the molecular ion H_3^+, which is stable with respect to dissociation into $H_2 + H^+$.[31] Such rings can be further stabilized by interaction with the d-orbitals of transition metals in organometallic sandwich compounds analogous to ferrocene.[31]

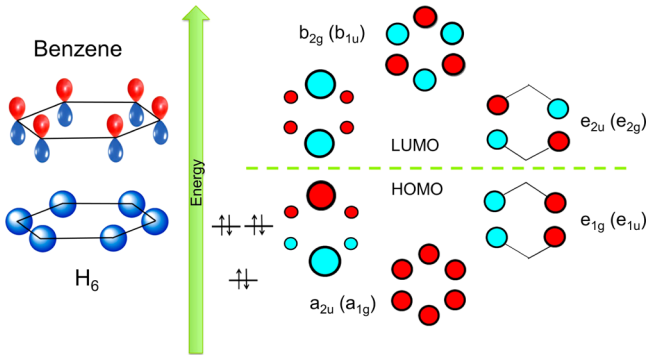

Figure 2. Symmetry-determined molecular orbitals in the H_6 ring and π orbitals in benzene. In the latter, the lowest energy molecular orbital is of a_{2u} symmetry and entirely bonding. The next two lowest energy orbitals are the mainly bonding e_{1g}, followed by the mainly antibonding e_{2u}. The b_{2g} orbital is entirely antibonding. The wave function coefficients for atomic $2p_z$ orbitals are reflected in the radius of the circle at each site, with the phase angle of 0 and $2\pi/3$ represented by red and cyan, respectively. In moving from benzene to H_6, the symmetry of the orbitals is changed as indicated in parentheses.

The stability of larger hydrogen rings were also examined, as early chemical models for metallic hydrogen. In particular, the calculations addressed the question of how many hydrogen atoms in H_n are needed to reproduce the cohesive energy and other properties of a hypothetical one-dimensional metallic hydrogen wire. Early *ab initio* calculations by Kislow et al.[33] investigated a series of closed-shell $4n + 2$ rings with 14, 26, 38, 50, and 62 hydrogen atoms. They found that H_{14} is a good representation of H_∞ if the accuracy demanded is 0.001 Å in bond distance and 0.0025 hartree (0.07 eV) in cohesive energy. When calculated self-consistently, the binding energy decreases with the number of atoms. Taking into account correlation energy, the result converges to that expected for one-dimensional metallic hydrogen (0.064 hartree or 1.73 eV per atom). The results confirmed the conclusion that aromatic rings of $n = 6$ and 10 atoms have the lowest binding energies among all of the rings.[31−33]

Meanwhile, early crossed molecular beam scattering experiments led Dixon et al.[22] to study in more detail the structural stability and chemical reactivity of H_6 rings.[22] This cluster was found to be the most stable form compared with three other symmetrical but nonplanar isomers: the octahedron (O_h), an eclipsed trigonal prism (D_{3h}) and a staggered trigonal prism (D_{3d}). Of the neutral H_{4n+2} rings, only H_6 is stable with respect to dissociation of one of the hydrogen molecules into two atoms: $H_{4n+2} \rightarrow 2nH_2 + 2H$. However, the cluster can dissociate into three H_2 molecules, its energy running smoothly downhill along the path associated with the B_{2u} or Kekulean vibrational mode.

In a prescient study, LeSar and Herschbach[23] considered the exceptional stability of six-atom rings in more detail, including at very high pressure. They predicted that molecular hydrogen transforms to a layered structure containing such rings at pressures above a few tens of gigapascals. This structure was suggested to contain hexagonal close-packed sites occupied by rings as if they were artificial atoms. Calculations based on semiempirical pair potentials were used to argue that the repulsion between the neighboring rings in the crystal environment prevents them from the dissociation into molecules. Though largely overlooked in subsequent theoretical work on hydrogen, related arguments for the stability of the hexagonal ring structures were advanced by Ashcroft[35] from the standpoint

dx.doi.org/10.1021/ar5002654 | Acc. Chem. Res. 2014, 47, 3551−3559

of solid-state physics. These early calculations[23,35] now have a special relevance to recent experimental results for hydrogen, including the mechanism of its pressure-induced metallization.

Chemical bonding effects of H_6 rings under pressure have been examined recently using more accurate methods by Labet et al.[12] The structural and electronic property changes of the cluster on compression were examined by varying the distance d from the center of symmetry to the centers of each of three H_2 molecules. With decreasing d, the intramolecular H−H distance elongates, whereas the intermolecular distance H_2−H_2 shortens, pushing the ring closer to D_{6h} symmetry. At the same time, the energy gap between HOMO and LUMO decreases, that is, the system becomes more "metallic". In the context of extended structures, such a mechanism of metallization corresponds to the overlapping between the bonding $1\sigma_g$ and antibonding $1\sigma_u^*$ states associated with 1s electrons only. As shown below, however, a more extended treatment of the same ring model indicates that both the 2s and 2p electrons are involved in the metallization.

Figure 3 shows the changes in total energy per atom with respect to the nearest separation for rings having D_{6h} symmetry calculated at different levels of theory, including both density functional theory with generalized gradient approximation corrections (DFT-GGA) and more sophisticated quantum chemistry methods with different basis sets.[34] At the DFT-GGA level, all rings except D_{3h} have a minimum energy at a separation close to 1 Å. In agreement with Hückel's rule, the $n = 6$ and $n = 10$ rings have the lowest total energies per atom and practically coincide (see also refs 31 and 32). The curves obtained from the quantum chemistry calculations have similar forms and equilibrium interatomic separations (see Supporting Information).

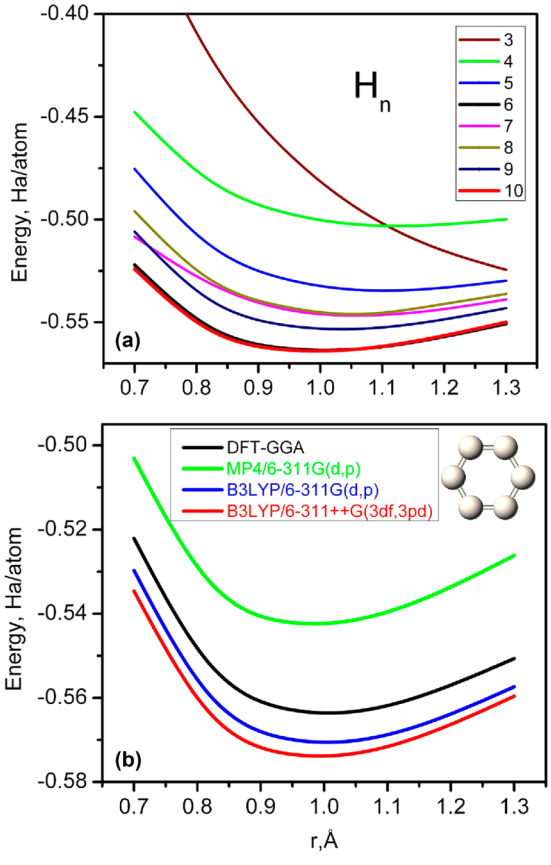

Figure 3. (a) Total energies per atom for H_n rings (n = 3−10) as a function of nearest atom separation. The n = 6 and 10 curves overlap. DFT-GGA results are shown; similar results are obtained at other levels of theory as shown in the Supporting Information. (b) Total energy versus nearest neighbor distance for the H_6 ring calculated using DFT-GGA and different quantum chemical methods: MP4/6-311G(d,p), B3LYP/6-311G(d,p), and B3LYP/6-311++G(3df,3dp) methods.[34] The latter calculations were performed with polarized basis sets containing p functions.

Comparing the curves for the H_6 ring shows that the DFT-GGA result lies somewhat above that calculated with the B3LYP hybrid functionals but far below the curve obtained within Hartree−Fock (HF)-derived MP4 approaches (Figure 3a). Similar results are found for HF, MP2, and QCISD calculations. Though correlation corrections considerably lower the total energy of a ring (especially in passing from HF to B3LYP), they have only little effect on its change with separation or in going to a different type of ring. Indeed, the HF to B3LYP calculations predict practically the same energy differences between different rings provided that the basis sets are identical (see Supporting Information). For different basis sets, however, the energy differences can be noticeable, in contrast to the optimized bond lengths (Table 1). The agreement between the different approaches, especially between the DFT-GGA and B3LYP-based methods, demonstrates that the key conclusions presented here are independent of the theoretical method used. The conclusions are also not affected by variations in the dispersion energy contribution,[36] which is relatively small for all calculations.

Table 1. Binding Energies (hartree/atom) of Hydrogen Rings at Optimized Bond Lengths

	MP4[a]		B3LYP[b]	
species	r (Å)	E (hartree)	r (Å)	E (hartree)
H_4	1.15	0.025	1.16	0.049
H_6	0.98	0.065	0.99	0.073
H_8	1.03	0.050	1.05	0.061

[a]MP4 calculations with 7 contracted functions per center.[31] [b]B3LYP/6-311G(d,p) calculations.

On the other hand, a notable difference between the two approaches is evident for the rings with odd number of atoms (electrons, i.e., n = 3, 5, and 7). In quantum chemistry, such rings are treated as open-shell systems. As a result, their energies tend to lie higher than those of the neighboring systems with $n - 1$ and $n + 1$ (Figure 4). In the contrasting solid-state (i.e., density functional) approach, the odd-electron rings are treated as effectively metallic systems, which ignores effects arising from unpaired electrons. Although the latter overestimates the stability of rings with odd electrons, the special "chemical" stability of aromatic systems with $4n + 2$ electrons is still captured in the solid-state physics approach.

DISTORTIONS AND DYNAMICAL STABILITY

The distortion of the ideal hydrogen hexagon (D_{6h}) toward a D_{3h} form with three long and three short H−H bonds is directly relevant to the high-pressure structures. The energetics of these clusters and the relative stability of H_n hydrogen ring structures are therefore examined in more detail. Of direct relevance to the recent high-pressure results are hydrogen rings having interatomic separations r between 1.10 and 0.90 Å: in extended 3D structures, these separations correspond to pressures of approximately 300−500 GPa.[12] Representative molecular energy

dx.doi.org/10.1021/ar5002654 | Acc. Chem. Res. 2014, 47, 3551−3559

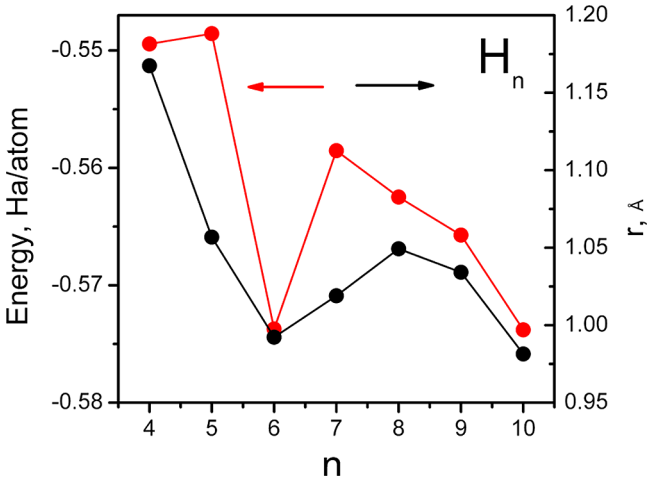

Figure 4. Total energy and optimized bond lengths in H_n rings for B3LYP/6-311G(d,p) calculations. The rings with odd n are assumed to be neutral and to have a spin multiplicity of 2.

levels and vibrational frequencies of H_6 as a function of separation r are shown in Figure 5.

Vibrational frequency calculations show that in its equilibrium configuration ($r \approx 1.00$ Å), the H_6 ring is unstable against the Kekulean (or B_{2u} vibrational) mode, in agreement with the previous work.[22,37] This mode distorts the initial D_{6h} geometry to a D_{3h} structure, ultimately transforming the hexagon into three H_2 molecules arranged in a triangular complex, as shown in the inset in Figure 5b. This D_{3h} structure captures a motif predicted for many candidate structures of compressed hydrogen.[15,16,18,19] As the distance r between the nearest atoms decreases, the driving force for the distortion weakens and the frequency of the mode becomes real for $r < 0.86$ Å. This distance corresponds to effective pressures of >500 GPa and reflects the tendency of the distorted graphene-like layers in dense hydrogen structures to be "more ideal" on compression.

As seen from Figure 5a, the character and relative positions of the LUMOs strongly depend on compression and can differ from that corresponding to the simple picture taking into account only minimum number of 1s basis functions (Figure 2). As the distance r decreases, the unoccupied 2s-derived bonding orbitals a_{1g} and e_{1u} quickly decrease in energy. Similar behavior is exhibited by the unoccupied bonding a_{2u} orbital that stems from the $2p_z$ atomic orbitals. As a result, for relatively small r, all three of these bonding molecular orbitals become lower in energy than the antibonding b_{1u} (and even e_{2g}) associated with the 1s electrons. As discussed further below, this fact is of principal importance for understanding the mechanism of metallization in extended structures of compressed hydrogen. We also point out that the calculated picture of the LUMOs in H_6 strongly depends on the chosen basis sets; the correct one is obtained only within the extended basis sets, which include 3p Gaussian functions on the hydrogen atoms [e.g., 6-331G(3df,3pd)] (see Supporting Information).

The distortive nature of the delocalized 1s electronic system of H_6 at relatively large separations is similar to that of the π-electronic system of benzene.[34] This phenomenon manifests itself for benzene in the sharp hardening of the B_{2u} vibrational mode upon excitation from the ground to its first B_{2u} excited electronic state.[38] The promotion of a π electron to an antibonding orbital reduces the π-distortion and increases the frequency of the Kekulean mode. In the case of H_6, the

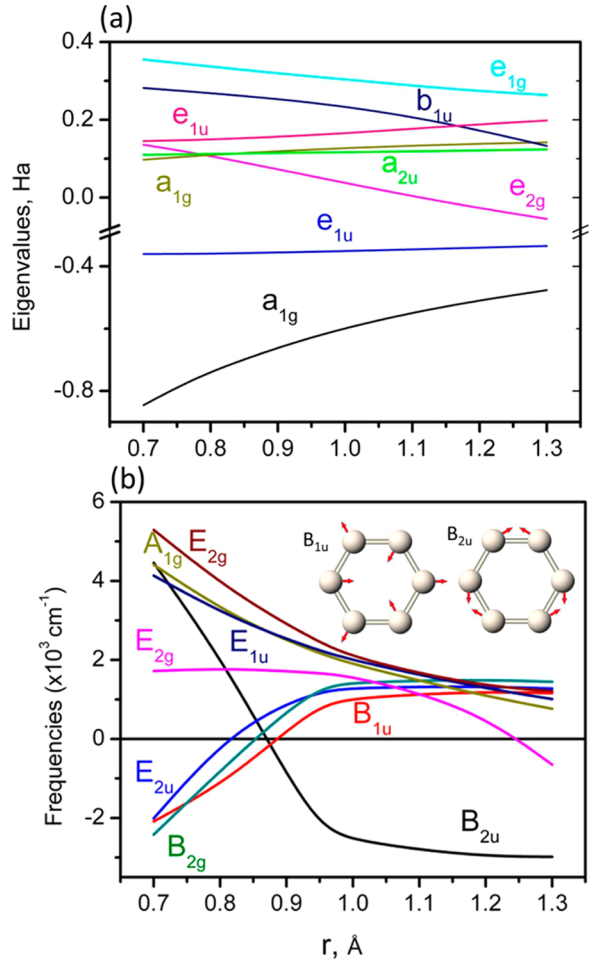

Figure 5. (a) Molecular energy levels and (b) vibrational frequencies as a function of separation r for the H_6 ring. The inset in panel b shows the vibrational displacements for B_{1u} and B_{2u} normal modes, which have the lowest and second-lowest energies at the equilibrium r of 1.00 Å. Negative frequencies represent the unstable modes and are the imaginary parts of ω [B3LYP/6-331G(3df,3pd) calculations].

stabilization of a D_{6h} structure against the B_{2u} distortion occurs not by the transfer of an electron but rather via hybridization with the gradual increase in 2s and 2p character of the bonding states at the expense of 1s character. This hybridization weakens the power of the 1s σ electrons to maintain a D_{3h} Kekulean structure and drives the system toward an ideal hexagon.

Though the H_6 ring becomes stable against the B_{2u} distortion for $r < 0.86$ Å, it becomes unstable relative to other three modes, B_{1u} , E_{2u} and B_{2g}, at these distances (Figure 5b; B_{1u} and B_{2u} are shown in the inset). In all of these modes, the atoms move in such a way as to increase the nearest separation and lower the total energy: the atoms repel each other to form a looser structure. The vibrational modes with the same symmetry (E_{2g}) strongly interact with each other when their frequencies cross near $r \approx 1$ Å. As a result, in accordance with the noncrossing rule, the high-frequency mode pushes the lower-frequency modes downward, and the latter becomes unstable for $r > 1.2$ Å along with B_{2u}.

Figure 6a shows the dependence of the total energy on the B_{2u} mode amplitude δ for $r = 0.90$ Å. Here, the amplitude δ is measured in terms of $2r/\sqrt{3}$, so that the shortest separation changes with δ as $r(1-\delta)$ and the longest as $r(1+\delta)$. The energy profile exhibits a shallow minimum at $\delta = 0.15$ corresponding to a nearest separation of 0.77 Å, which is somewhat less than the

dx.doi.org/10.1021/ar5002654 | Acc. Chem. Res. 2014, 47, 3551−3559

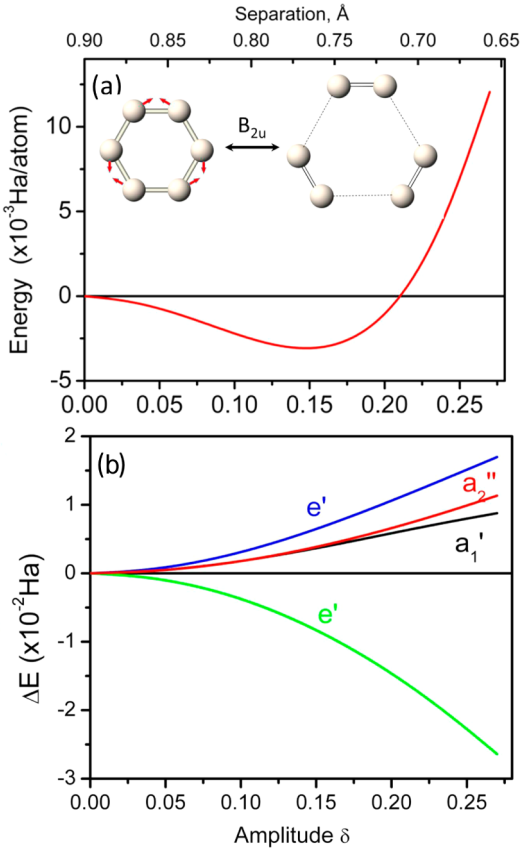

Figure 6. Energetics of the H_6 hexagon with respect to the B_{2u} vibrational mode: (a) energy and (b) eigenvalues. An initial bond length of 0.90 Å was used, and the amplitude is measured in $2r/\sqrt{3}$, so that the nearest distance between hydrogen atoms is $r(1-\delta)$. The initial molecular levels correspond to $\delta = 0$. All results are obtained at the B3LYP/6-331G(3df,3pd) level of calculation.

bond length in isolated H_2 (0.74 Å). With decreasing initial bond length r, the minimum becomes progressively shallower, and for r < 0.86 Å, it completely disappears, in accordance with the results shown in Figure 4. Before this critical point (for larger r), the depth of the energy well is very shallow, being only about 2×10^{-3} hartree for r = 0.90 Å.

As δ increases, the energy gap between the LUMO and HOMO widens (Figures 6b,c). Indeed, the bonding (e′) and antibonding (both e′) orbitals decrease and increase in energy, respectively. At the same time, the energy of the bonding a_2'' term decreases relative to the antibonding level e′. The shapes of the orbitals and their changes with δ are shown in Figure 7. It is seen that the closed-shell electronic structure does not change with δ or in passing from a D_{6h} to D_{3h} ring. Thus, the latter remains aromatic. One can also clearly see that the second-lowest unoccupied orbitals a_{2u} (a_2'') are bonding and stem from the atomic $2p_z$ orbitals. This result contrasts with that reported in ref 12 where they are antibonding and 1s-derived, a discrepancy that can be attributed to a different choice of basis sets. As mentioned above, the symmetry of the unoccupied orbitals is very sensitive to such choices.

FROM ISOLATED RINGS TO TWO DIMENSIONAL SHEETS

We proceed from H_n rings to periodic networks of such rings in two-dimensional lattices. Since the crystal lattice can have axes of symmetry only of order 2, 3, 4, and 6, we can use only H_3, H_4, and H_6 to build triangle, square, and graphene-like lattices, respectively. The graphene-like structure with the optimized lattice parameter is far more favorable energetically than the other two (Table 2). For this structure, the energy versus r curve exhibits a comparatively sharp minimum at r = 1.18 Å. In contrast, the corresponding profiles in triangle and square lattices are characterized by shallow minima that emerge for r > 4 Å.

Table 2. Optimized Bond Lengths and Energies Per Atom for Hydrogen Rings and Two-Dimensional Hydrogen Lattices

	r (Å)	E (Ha)	ΔE^a (Ha)
triangle	4.23	−0.451	0.075
square	4.35	−0.451	0.052
graphene-like	1.18	−0.555	0.009

[a] ΔE is the change in energy in progressing from a ring to the corresponding lattice (DFT-GGA calculations).

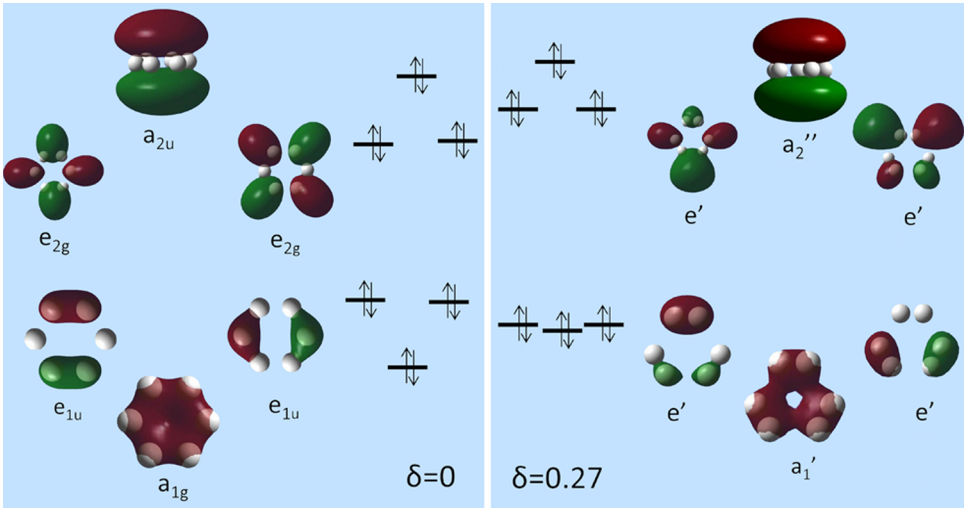

Figure 7. Correlation between the molecular orbitals for $\delta = 0$ (D_{6h}) and $\delta = 0.27$ (D_{3h}) structures. As in Figure 5, the initial bond length is 0.90 Å. The orbitals are labeled according to D_{6h} and D_{3h} point group symmetries, respectively.

dx.doi.org/10.1021/ar5002654 | Acc. Chem. Res. 2014, 47, 3551−3559

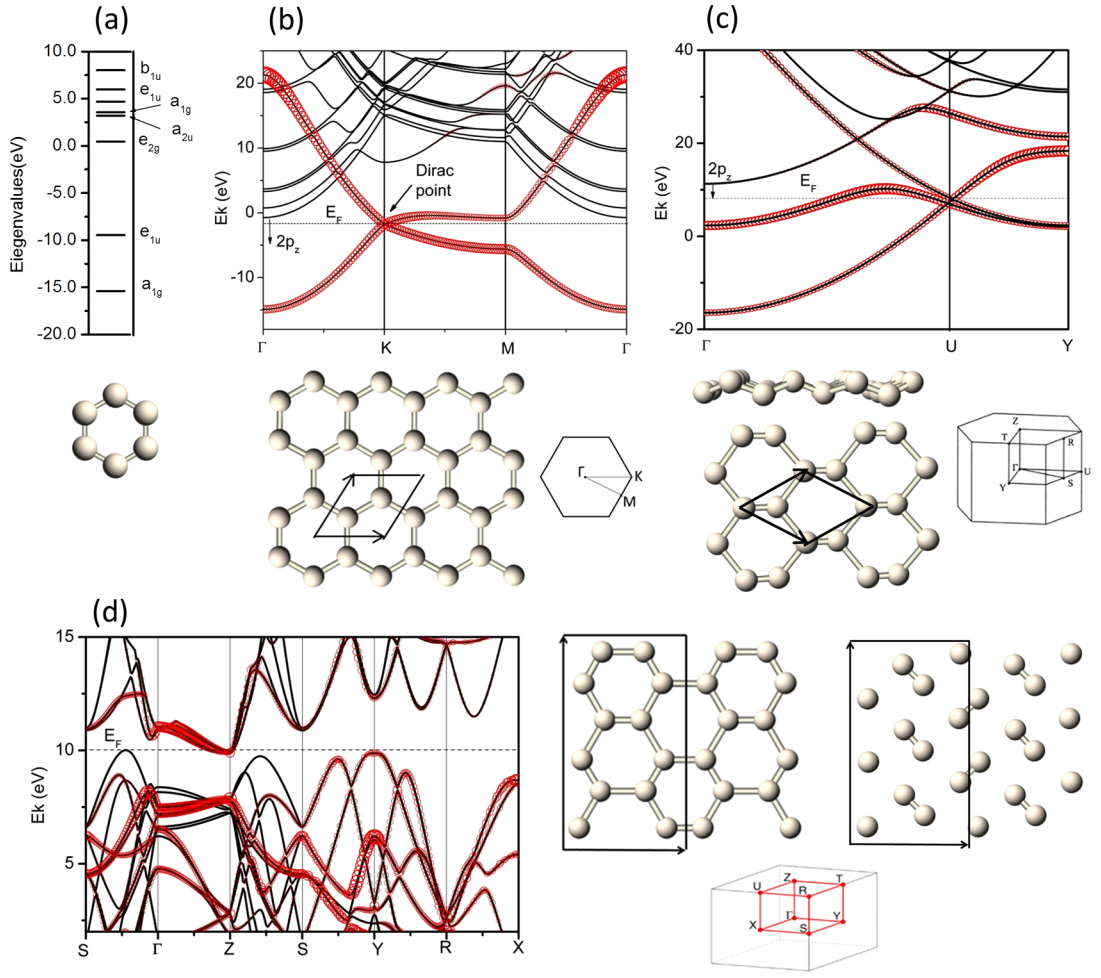

Figure 8. Evolution of electronic structure on passing from the H_6 ring to 2D graphene layer and to a 3D model structure. (a) Energy level diagram in H_6 ring for an equilibrium bond length of 1.00 Å [B3LYP/6-331G(3df,3pd) calculation]. (b) DFT-GGA band structure for H-graphene with a equilibrium bond length of 1.177 Å. (c) Band structure for the orthorhombic *Cmca*-4 phase at 300 GPa. Each layer in *Cmca*-4 can be viewed as a buckled graphene layer consisting of H_2 molecules tilted relative to the *xy* plane; the side and top views of such a layer are depicted. (d) Band structure for the orthorhombic *Pbcn* phase at 300 GPa. In this structure, the graphene-like layers (A and C) and layers of weakly interacting H_2 molecules (B and D) are stacked in the fashion ABCD. Only A and B layers are depicted. The 1s character of the wave functions, which is proportional to the size of red circles or thickness of the curves, is shown.

Upon formation of lattices from the corresponding rings, the energy per atom increases only modestly for the graphene-like lattice but shows a pronounced increase for the triangle and square lattices.

Upon fusion of H_6 rings in a graphene layer, the initial molecular orbitals overlap and the molecular levels evolve into valence and conduction energy bands. If $r > 1.1$ Å (up to a critical value) in each constituent hexagon, the valence band originating from the a_{1g} and e_{1u} orbitals and the conduction band stemming from the e_{2g} and b_{1u} orbitals touch at two inequivalent Dirac points, K and K'[18,19] (Figure 8b). These states are mainly of 1s character, which is quantitatively expressed by the thickness of the line (red circles). We find that it is the overlap between the bonding $1\sigma_g$ and antibonding $1\sigma_u$* bands that is responsible for the formation of the semimetallic zero-gap phase. Such a structure has a vanishing density of states at the Fermi level. However, not all the conduction states near the Fermi level are 1s-derived, especially in the vicinity of the Γ point. The next energy level at Γ is the bottom of the bonding $2p_z$ band, which is genetically connected with the a_{2u} level corresponding to the second-lowest unoccupied orbital in the H_6 ring for Γ close to 1 Å (see Figure 8a). Like a_{2u}, the former rapidly moves downward as the lattice parameter decreases, and drops below the Dirac level at $r = 1.1$ Å. The resulting band structure corresponds to a new semimetallic phase with a finite density of states at the Fermi level. As the lattice parameter decreases further, the third energy term at Γ decreases and crosses the Fermi level, leading to a more complex semimetallic phase for the H_6 sheet. As the analysis shows, this term is directly connected with the 2s-derived a_{1g} orbital of H_6.

FROM TWO DIMENSIONAL SHEETS TO THREE DIMENSIONAL STRUCTURES

We now move from ideal hydrogen 2D networks to 3D structures. Many candidate structures proposed for dense hydrogen, such as *C*2/*c*, *Pbcn*, *Cc*, *Pc*, and *Cmca*-4, can be modeled as consisting of distorted graphene sheets.[19] To elucidate the evolution of the chemical bonding in going from 2D sheets to 3D structures, we choose two orthorhombic structures as prototypes, labeled by the following space groups: *Pbcn*, which is considered a model structure for phase IV, and *Cmca*-4, which is predicted to exist at higher pressures (e.g., >370 GPa) (e.g., ref 11). Geometrically, these are layered structures

dx.doi.org/10.1021/ar5002654 | *Acc. Chem. Res.* 2014, 47, 3551−3559

arranged in ABCD and AB sequences, respectively. In *Pbcn*, the graphene-like layers, A and C, are sandwiched between the layers of weakly interacting H_2 molecules, B and D; each layer contains 12 atoms. *Cmca*-4 is close to the graphite-type structure where the honeycomb layers are also arranged in an AB stacking sequence (Bernal order). It should be stressed that the layers in both prototype phases are not ideally flat but buckled, especially in *Cmca*-4 (Figure 8c) where the H_2 molecules form an angle $\theta \approx 30^\circ$ with respect to the *xy* plane. By close analogy, graphite[29] itself, as well as hydrogen in both the *Pbcn* and *Cmca*-4 structures, can also be considered as aromatic. This is evident by considering polycyclic aromatic hydrogen clusters of increasing size starting with ideal or distorted H_6 rings (plus aromatic H_2 molecules in the case of *Pbcn*).

Figure 8c presents the band structure for *Cmca*-4 calculated at 300 GPa. Its close relationship to that for hydrogenic graphene (and the H_6 rings) can be easily understood. Indeed, in the *Cmca*-4 structure there are four atoms per cell, instead of two in the graphene layer. In solid-state physics terms, the Γ−U line in the orthorhombic Brillouin zone is an analog of the Γ−K direction in the hexagonal zone. Moreover, the four lowest energy bands in the vicinity of U are analogous to the two lowest bands in graphene in the vicinity of K. They also have mainly 1s character because they originate from mixing the 1s-derived layer states. Similar to the case of graphene, here the 1s-derived bands are not the only states near the Fermi level. As in graphene, the bonding $2p_z$ band quickly moves down (especially near Γ) with pressure and passes the Fermi level just above 300 GPa. This band is strongly hybridized with the 1s orbitals due to tilting of the H_2 pairs with respect to the basal plane.

In contrast to *Cmca*-4, the *Pbcn* structure exhibits insulating behavior (Figure 8d). Such a difference can be explained by the fact that each graphene-like layer in *Pbcn* can be considered as a 3×2 superlattice stabilized by Peierls-like distortions that open an energy gap in an ideal honeycomb layer by mixing the Dirac *K* and *K*′ states. An additional contribution to the "dielectrization" of the electronic spectrum comes from the $1s-2p_z$ mixing due to tilting of the H_2 pairs, similar to the case of *Cmca*-4. It is clear that both the Peierls distortions and molecular tilting further strengthen closed-shell effects, which decrease the total energy. The examples considered show that the band structures of the layered 3D structures can be understood in terms of the constituent H_6 rings and H_n graphene sheets.

DISCUSSION AND OUTLOOK

The stability of the structures of dense solid hydrogen at megabar pressures can be understood in terms of closed shell effects that are well-known in chemistry. In particular, H_6 rings and graphene-like sheets of the H_n rings, H_6, and its larger analogs (H_{4n+2}, $n > 1$) are especially stable due to aromatic and closed-shell effects. To exhibit such stability, the H_6 system need not have an ideal bond-equalized geometry (i.e., D_{6h} symmetry) but only have cyclical conjugation. Indeed, the six-membered rings with D_{3h} symmetry are generally more stable than their D_{6h} counterparts at various levels of theory. The situation is analogous to that in benzene where the π contribution to C−C bonding becomes stabilizing when the geometry is distorted toward D_{3h}.[36]

In this chemical picture of hydrogen metallization, the transition proceeds via the formation of bonding states with 2s σ and $2p_z$ π character, which correlate with the LUMOs of H_6. These states become the dominant component of the lowest conduction bands in hydrogenic graphene and real bulk structures observed experimentally and calculated theoretically. Under pressure at some point, the bottoms of these bands become lower in energy than the Fermi level (and antibonding bands associated with 1s electrons), thus giving rise to a semiconductor−semimetallic transition. As the calculations show, on compression, the bonding $2p_z$ π bands pass the Fermi level earlier than their 2s σ counterparts. The reason is that the kinetic energy contribution to the one-electron eigenvalues becomes larger than the potential energy contribution.[39] As a result, the orbitals with fewer nodes in their radial wave functions such as the 2p (with none) are more favorable than those such as 2s (with one).

Similar to H_6 rings, the hydrogenic graphene-like sheets represent aromatic systems but are of the extended type. This closely parallels real (carbon) graphene, the stability of which can be explained by considering polycyclic aromatic hydrocarbons of increasing size starting with benzene.[30] As for H_6 rings, a hydrogenic aromatic sheet need not have an ideal honeycomb lattice with D_{6h} point symmetry. In fact, distortions of the ideal structure reduce the energy of this system further and make it even more "aromatic." These possibilities include Peierls-like distortions that mix the unperturbed *K* and *K*′ Bloch states and open a gap leading to the formation of superlattices with multiples of 3 or $\sqrt{3}$.[18,19] Indeed, one such distortion is of the Kekulean type, which also strengthens the H_6 stability, as shown above.

In the high-pressure hydrogen structures,[10−19] the minimum distance between two hydrogen atoms from neighboring layers is noticeably shorter than the intermolecular distance in the graphene-like layers. Thus, the enhanced chemical stability of these structures is also associated with aromaticity. The situation is similar to that occurring when passing from carbon graphene to graphite. As for graphene, graphite is considered aromatic because of the relatively large separation between the layers compared with the distance between atoms within the layer. Indeed, graphite is considered even more aromatic than benzene, having a higher resonance energy per π electron.[29] A measure of the aromacity of graphite is its large negative magnetic susceptibility χ.[40] By analogy to graphite, one can expect dense solid hydrogen also to be strongly diamagnetic, with layered structures characterized by a sharp rise in χ, especially in its out-of-plane component χ_{zz}.

Similar in Hume−Rothery phases or quasicrystals, the closed shell effects in 3D compressed hydrogen structures are associated with the "dielectrization" of the electronic spectrum.[41] As such, they compete with metallization, that is, the classic pressure-induced insulator−metal transition.[21] In hydrogen at high densities, the electronic and atomic degrees of freedom are closely interconnected, and the system finds a variety of ways to open a gap, that is, through the Peierls-like distortions, 1s−2p hybridization and tilting of the H_2 pairs, and other distortions.[19] The parallels discussed above have implications for further experimental characterization of dense hydrogen. In particular, given the diamagnetic character expected for the graphene-based structures, modern high-pressure magnetic susceptibility measurements may supplement magnetic probes of other novel electronic properties such as the predicted superconductivity of the material.[42,43]

dx.doi.org/10.1021/ar5002654 | *Acc. Chem. Res.* 2014, 47, 3551−3559

■ ASSOCIATED CONTENT

Supporting Information

Additional comparisons between the quantum chemical and density-function results, including changes in energy levels with interatomic distance. This material is available free of charge via the Internet at http://pubs.acs.org.

■ AUTHOR INFORMATION

Corresponding Author

*Russell J. Hemley. E-mail: rhemley@ciw.edu.

Author Contributions

‡These authors contributed equally.

Notes

The authors declare no competing financial interest.

Biographies

Ivan Naumov was born on September 3, 1952, in Tyumen Region, Russia. He is currently a Research Scientist at the Geophysical Laboratory, Carnegie Institution of Washington. He received his M.S. and Ph.D. from Tomsk State University in 1974 and 1980, respectively, and then worked at the Institute of Strength Physics and Materials Science of the Russian Academy of Sciences, where he earned Doctor of Physical and Mathematical Sciences and also served as a professor at Tomsk State University. From 2007 to 2012, he worked at Hewlett-Packard Laboratories. His research interests include a broad array of structural, electronic, vibrational, and transport properties of materials such as ferroelectrics, superconductors, shape-memory alloys, and graphene-based nanostructures. His most recent studies are focused on highly compressed materials including hydrogen.

Russell J. Hemley was born on October 26, 1954, in Berkeley, CA. He received his B.A. from Wesleyan University (1977) and did his graduate work in physical chemistry at Harvard University (M.A., 1980; Ph.D. 1983). After a post-doctoral fellowship at Harvard (1983−1984), he joined the Geophysical Laboratory as a Carnegie Fellow (1984−1986) and Research Associate (1986−1987). He became a Staff Scientist in 1987 and served as Director of the Geophysical Laboratory from 2007 to 2013. His research explores the chemistry of materials over a broad range of thermodynamic conditions from low to very high pressures with application to condensed matter physics, earth and planetary science, and materials science. He is a Fellow of the American Academy of Arts and Sciences, Member of the National Academy of Sciences (2001), Corresponding Fellow of the Royal Society of Edinburgh (2008), and Honoris Causa Professor of the Russian Academy of Sciences (2008).

■ ACKNOWLEDGMENTS

This research was supported by EFree, an Energy Frontier Research Center funded by the U.S. Department of Energy, Office of Science, Basic Energy Sciences under Award DE-SC0001057. The infrastructure and facilities used are supported by U.S. National Science Foundation (Grant DMR-1106132) and the U.S. Department of Energy/National Nuclear Security Administration (Grant DE-NA-00006, CDAC).

■ REFERENCES

(1) Lewis, G. N. The Atom and the Molecule. *J. Am. Chem. Soc.* **1916**, *38*, 762−785.

(2) Luh, D. A.; Miller, T.; Paggel, J. J.; Chou, M. Y.; Chiang, T. C. Quantum Electronic Stability of Atomically Uniform Films. *Science* **2001**, *292*, 1131−1133.

(3) Yanson, A. I.; Yanson, I. K.; van Ruitenbeek, J. M. Observation of Shell Structure in Sodium Nanowires. *Nature* **1999**, *400*, 144−146.

(4) Kroto, H. W.; Heath, J. R.; O'Brien, S. C.; Curl, R. F.; Smalley, R. E. C_{60}: Buckminsterfullerene. *Nature* **1985**, *318*, 162−163.

(5) Heitler, W.; London, F. Wechselwirkung Neutraler Atome und Homöopolare Bindung nach der Quantenmechanik. *Z. Phys.* **1927**, *44*, 455−472.

(6) Pauling, L. *The Nature of the Chemical Bond*; Cornell University Press: Ithaca, NY, 1960.

(7) Hirschfelder, O.; Curtiss, C. F.; Bird, R. B. *Molecular Theory of Gases and Liquids*; Wiley: New York, 1954.

(8) Grochala, W.; Hoffmann, R.; Feng, J.; Ashcroft, N. W. The Chemical Imagination at Work in Very Tight Places. *Angew. Chem., Int. Ed.* **2007**, *46*, 3620−3642.

(9) Hemley, R. J. Percy Bridgman's Second Century. *High Press. Res.* **2010**, *30*, 581−619.

(10) Eremets, M. I.; Troyan, I. A. Conductive Dense Hydrogen. *Nat. Mater.* **2011**, *10*, 927−931.

(11) Howie, R. T.; Guillaume, C. L.; Scheler, T.; Goncharov, A. F.; Gregoryanz, E. Mixed Molecular and Atomic Phase of Dense Hydrogen. *Phys. Rev. Lett.* **2012**, *108*, No. 125501.

(12) Labet, V.; Gonzalez-Morelos, P.; Hoffmann, R.; Ashcroft, N. W. A Fresh Look at Dense Hydrogen under Pressure. I. An Introduction to the Problem, and an Index Probing Equalization of H−H Distances. *J. Chem. Phys.* **2012**, *136*, No. 074501.

(13) Liu, H.; Ma, Y. Proton or Deuteron Transfer in Phase IV of Solid Hydrogen and Deuterium. *Phys. Rev. Lett.* **2013**, *110*, No. 025903.

(14) Liu, H.; Zhu, L.; Cui, W.; Ma, Y. Room-Temperature Structures of Solid Hydrogen at High Pressures. *J. Chem. Phys.* **2012**, *137*, No. 074501.

(15) Pickard, C. J.; Martinez-Canales, M.; Needs, R. J. Density Functional Theory Study of Phase IV of Solid Hydrogen. *Phys. Rev. B* **2012**, *85*, No. 214114; Erratum: Density functional theory study of phase IV of solid hydrogen [Phys. Rev. B **85**, 214114 (2012)]. *Phys. Rev. B* **2012**, *86*, No. 059902.

(16) Pickard, C. J.; Needs, R. J. Structure of Phase III of Solid Hydrogen. *Nat. Phys.* **2007**, *3*, 473−476.

(17) Zha, C. S.; Liu, Z.; Ahart, M.; Boehler, R.; Hemley, R. J. High-Pressure Measurements of Hydrogen Phase IV Using Synchrotron Infrared Spectroscopy. *Phys. Rev. Lett.* **2013**, *110*, No. 217402.

(18) Cohen, R. E.; Naumov, I. I.; Hemley, R. J. Electronic Excitations and Metallization of Dense Solid Hydrogen. *Proc. Natl. Acad. Sci. U.S.A.* **2013**, *110*, 13757−13762.

(19) Naumov, I. I.; Cohen, R. E.; Hemley, R. J. Graphene Physics and Insulator-Metal Transition in Compressed Hydrogen. *Phys. Rev. B* **2013**, *88*, No. 045125.

(20) Azadi, S.; Foulkes, W. M. C.; Kühne, T. D. Quantum Monte Carlo Study of High Pressure Solid Molecular Hydrogen. *New J. Phys.* **2013**, *15*, No. 113005.

(21) Wigner, E.; Huntington, H. B. On the Possibility of a Metallic Modification of Hydrogen. *J. Chem. Phys.* **1935**, *3*, 764−770.

(22) Dixon, D. A.; Stevens, R. M.; Herschbach, D. R. Potential Energy Surface for Bond Exchange among Three Hydrogen Molecules. *Faraday Discuss. Chem. Soc.* **1977**, *62*, 110−126.

(23) LeSar, R.; Herschbach, D. R. Likelihood of a High-Pressure Phase of Solid Hydrogen Involving Termolecular Complexes. *J. Phys. Chem.* **1981**, *85*, 3787−3792.

(24) Taylor, P. R.; Komornicki, A.; Dixon, D. A. Ab Initio CI Treatment of the Termolecular Reaction of $3H_2$: Hexagonal H_6. *J. Am. Chem. Soc.* **1989**, *111*, 1259−1262.

(25) Novoselov, K. S.; Geim, A. K.; Morozov, S. V.; Jiang, D.; Zhang, Y.; Dubonos, S. V.; Grigorieva, I. V.; Firsov, A. A. Electric Field Effect in Atomically Thin Carbon Films. *Science* **2004**, *306*, 666−669.

(26) Shaik, S.; Hiberty, P. C. *A Chemist's Guide to Valence Bond Theory*; John Wiley and Sons, Inc.: Hoboken, NJ, 2008.

(27) Hiberty, P. C.; Shaik, S. Some Answers to Frequently Asked Questions about the Distortive Tendencies of π-Electronic System. *Theor. Chem. Acc.* **2005**, *114*, 169−181.

(28) Mao, H. K.; Hemley, R. J. Ultrahigh Pressure Transitions in Solid Hydrogen. *Rev. Mod. Phys.* **1994**, *66*, 671−692.
(29) Moran, D.; Stahl, F.; Bettinger, H. F.; Schaefer, H. F.; Schleyer, P. V. R. Towards Graphite: Magnetic Properties of Large Polybenzenoid Hydrocarbons. *J. Am. Chem. Soc.* **2003**, *125*, 6746−6752.
(30) Popov, I. A.; Bozhenko, K. V.; Boldyrev, A. I. Is Graphene Aromatic? *Nano Res.* **2012**, *5*, 117−123.
(31) Wright, J. S.; DiLabio, G. A. Structure and Stability of Hydrogen Rings. *J. Phys. Chem.* **1992**, *96*, 10793−10799.
(32) Ichikawa, H. On the Stability of the Polygonal H_n Systems. Simple Models of Aromaticity and Antiaromaticity. *J. Am. Chem. Soc.* **1983**, *105*, 7467−7468.
(33) Kislow, D. H.; McKelvey, J. M.; Bender, C. F.; Schaefer, H. F. *A Priori* Prediction of the Cohesive Energy of One-Dimensional Metallic Hydrogen. *Phys. Rev. Lett.* **1974**, *32*, 933−936.
(34) Frisch, M. J.; Trucks, G. W.; Schlegel, H. B.; Scuseria, G. E.; Robb, M. A.; Cheeseman, J. R.; Scalmani, G.; Barone, V.; Mennucci, B.; Petersson, G. A.; Nakatsuji, H.; Caricato, M.; Li, X.; Hratchian, H. P.; Izmaylov, A. F.; Bloino, J.; Zheng, G.; Sonnenberg, J. L.; Hada, M.; Ehara, M.; Toyota, K.; Fukuda, R.; Hasegawa, J.; Ishida, M.; Nakajima, T.; Honda, Y.; Kitao, O.; Nakai, H.; Vreven, T.; Montgomery, J. A., Jr.; Peralta, J. E.; Ogliaro, F.; Bearpark, M.; Heyd, J. J.; Brothers, E.; Kudin, K. N.; Staroverov, V. N.; Kobayashi, R.; Normand, J.; Raghavachari, K.; Rendell, A.; Burant, J. C.; Iyengar, S. S.; Tomasi, J.; Cossi, M.; Rega, N.; Millam, J. M.; Klene, M.; Knox, J. E.; Cross, J. B.; Bakken, V.; Adamo, C.; Jaramillo, J.; Gomperts, R.; Stratmann, R. E.; Yazyev, O.; Austin, A. J.; Cammi, R.; Pomelli, C.; Ochterski, J. W.; Martin, R. L.; Morokuma, K.; Zakrzewski, V. G.; Voth, G. A.; Salvador, P.; Dannenberg, J. J.; Dapprich, S.; Daniels, A. D.; Farkas, O.; Foresman, J. B.; Ortiz, J. V.; Cioslowski, J.; Fox, D. J. *Gaussian 09*, revision D.01; Gaussian, Inc.: Wallingford, CT, 2009.
(35) Ashcroft, N. W. Optical Response Near a Band Overlap: Application to Dense Hydrogen. In *Molecular Systems under High Pressures*; Pucci, R., Piccitto, G., Eds.; Elsevier: Amsterdam, 1991; pp 201−222.
(36) Pykko, P. Strong Closed-Shell Interactions in Inorganic Chemistry. *Chem. Rev.* **1997**, *97*, 597−636.
(37) Najafpour, J.; Foroutan-Nejad, C.; Shafiee, G. H.; Peykani, M. K. How Does Electron Delocalization Affect the Electronic Energy? A Survey of Neutral Poly-nitrogen Clusters. *Comput. Theor. Chem.* **2011**, *974*, 86−91.
(38) Shechtman, D.; Blech, I.; Gratias, D.; Cahn, J. W. Metallic Phase with Long-Range Orientational Order and No Translational Symmetry. *Phys. Rev. Lett.* **1984**, *53*, 1951−1953.
(39) McMahan, A. K. Pressure-Induced Changes in the Electronic Structure of Solids. *Physica B+C* **1986**, *139−140*, 31−41.
(40) Cyranski, M. K. Energetic Aspects of Cyclic Pi-Electron Delocalization: Evaluation of the Methods of Estimating Aromatic Stabilization Energies. *Chem. Rev.* **2005**, *105*, 3773−3811.
(41) Fortov, V. E.; Mintsev, V. B. Extreme States of Matter on the Earth and in the Cosmos: Is There Any Chemistry beyond the Megabar? *Russ. Chem. Rev.* **2013**, *82*, 597−615.
(42) Richardson, C. F.; Ashcroft, N. W. High Temperature Superconductivity in Metallic Hydrogen: Electron-Electron Enhancements. *Phys. Rev. Lett.* **1997**, *78*, 118−121.
(43) Cudazzo, P.; Profeta, G.; Sanna, A.; Floris, A.; Continenza, A.; Massidda, S.; Gross, E. K. U. Ab Initio Description of High-Temperature Superconductivity in Dense Molecular Hydrogen. *Phys. Rev. Lett.* **2008**, *101*, No. 029901.